Journal of Power Sources 256 (2014) 190–199

Contents lists available at ScienceDirect

Journal of Power Sources

journal homepage: www.elsevier.com/locate/jpowsour

High performance amorphous-Si@SiO_x/C composite anode materials for Li-ion batteries derived from ball-milling and in situ carbonization

Dingsheng Wang, Mingxia Gao*, Hongge Pan*, Junhua Wang, Yongfeng Liu

State Key Laboratory of Silicon Materials, Key Laboratory of Advanced Materials and Applications for Batteries of Zhejiang Province & Department of Materials Science and Engineering, Zhejiang University, Hangzhou 310027, PR China

HIGHLIGHTS

- Amorphous Si (a-Si) powder with SiO_x surface layer introduced is prepared by ball-milling.
- Carbon coating and floc-like carbon are introduced in situ in the a-Si@SiO_x particles.
- The a-Si@SiO_x/C composite with 8 wt.% C provides superior electrochemical performance.
- The method is facile in large-scale production of Si-based anode material for LIBs.

ARTICLE INFO

Article history:
Received 7 November 2013
Received in revised form
20 December 2013
Accepted 29 December 2013
Available online 20 January 2014

Keywords:
Lithium-ion batteries
Anode
Ball milling
Amorphous silicon
Silicon protoxide
Carbon

ABSTRACT

Amorphous-Si@SiO_x/C composites with amorphous Si particles as core and coated with a double layer of SiO_x and carbon are prepared by ball-milling crystal micron-sized silicon powders and carbonization of the citric acid intruded in the ball-milled Si. Different ratios of Si to citric acid are used in order to optimize the electrochemical performance. It is found that SiO_x exists naturally at the surfaces of raw Si particles and its content increases to *ca.* 24 wt.% after ball-milling. With an optimized Si to citric acid weight ratio of 1/2.5, corresponding to 8.4 wt.% C in the composite, a thin carbon layer is coated on the surfaces of a-Si@SiO_x particles, moreover, floc-like carbon also forms and connects the carbon coated a-Si@SiO_x particles. The composite provides a capacity of 1450 mA h g^{-1} after 100 cycles at a current density of 100 mA g^1, and a capacity of 1230 mA h g^{-1} after 100 cycles at 500 mA g^1 as anode material for lithium-ion batteries. Effects of ball-milling and the addition of citric acid on the microstructure and electrochemical properties of the composites are revealed and the mechanism of the improvement in electrochemical properties is discussed.

1. Introduction

The property of lithium-ion batteries (LIBs) has been considerably enhanced in recent years. However, further improvement is still necessary to realize their application in the highly desired high-energy density power sources used for hybrid, plug-in hybrid electric vehicles and the energy storage systems for wind and solar energies, and so on. Although graphite is still the commercially dominant anode material for LIBs until now, its limited theoretic capacity (372 mA h g^{-1}) cannot meet fully the requirement of the high-energy density power sources. Silicon is one of the most promising alternative anode material of next-generation due to its high theoretical capacity (4200 mA h g^{-1} corresponding to the fully lithiated composition of $Li_{4.4}Si$), attractive voltage profile, abundance and low cost. However, the practical use of silicon anode is hindered by its low intrinsic electric conductivity and severe volume changes (>300%) during lithiation/delithiation processes [1,2], which lead to its low cycle stability. The main approaches explored to overcome these two disadvantages include: (1) designing nano-sized materials, such as nanoparticles, Si nanowires, Si nanotubes, etc. [3–5], and porous materials [6,7], to decrease the huge volume change; (2) combining inactive/less active materials, such as metal alloys [8,9] and metal oxides [10,11] to buffer the large volume change; (3) introducing carbonaceous materials to form Si/C composites, which can both increase the electrical conductivity and buffer partially the volume change of Si [12–14]. In addition, using

* Corresponding authors. Tel./fax: +86 571 87952615.
E-mail addresses: gaomx@zju.edu.cn (M. Gao), hgpan@zju.edu.cn (H. Pan).

0378-7753/$ – see front matter © 2014 Elsevier B.V. All rights reserved.
http://dx.doi.org/10.1016/j.jpowsour.2013.12.128

suitable binders [3,15] to get solid bond of the particles is also effective in improving the electrochemical properties of the Si-based anodes.

Nano-sized and porous materials can offer high reversible capacity and cycle stability. However, they have a common drawback of low packing density and thus low volumetric energy density. In addition, nano-sized materials are generally of low-yield and high-cost, and have high surface tension. Nanostructuring of micro-scale electrode materials is considered as an effective solution to increase the volumetric energy density [16]. For Si/C composites, different types of carbons are used and various methods are investigated, such as the external introduction of carbon nanofibers (CNFs) in Si particles [13], coating amorphous silicon layers via chemical vapor deposition (CVD) on both the exterior and interior surfaces of the hollow carbon nanofibers [17], preparing carbon-coated nano-crystalline Si composites by spray-pyrolysis [18].

In terms of Si, both crystal Si (c-Si) and a-Si are lithium reaction active. However, a-Si provides more paths for the insertion/extraction of lithium [4,19–22], and the volume expansion of a-Si upon lithium insertion is isotropic, which causes less pulverization compared with the highly anisotropic expansion of c-Si [23]. One method to fabricate a-Si is deposition, such as plasma deposition [6] and CVD [14]. Amorphous Si/C nano-spheres with a diameter of 400–600 nm were obtained by a CVD method using methyltrichlorosilane (CH_3SiCl_3) as both the Si and C sources [14]. The method is considered of low-cost. However, the capacity of this Si/C composite is barely above that of the commercial graphite within 50 cycles. An intercalated a-Si/C film with a critical thickness of 20 nm Si layer and C layer prepared by dual plasma deposition shows superior electrochemical property, however, the synthesis process is expensive and the volumetric capacity of the film anode is limited [7]. Ball milling is considered to be an effective approach to obtain powder materials with nano-crystallite and even amorphous structure, which is also favorable for large scale production. It is reported that ball milling micro-size crystal Si can produce nano-crystallite micro-Si [24] and amorphous Si [25], the cycle stability of which are all effectively improved.

In addition, SiO_2, or strictly, SiO_x (silicon protoxide, $x < 2$), forms readily at the surface of Si particles at atmosphere environment. Bulk SiO_2 is generally considered inactive for electrochemical lithium storage. However, nano-structured or amorphous SiO_2 is lithium reactive [11,26]. The theoretical specific capacity of SiO_2 is calculated to be 1965 mA h g^{-1} when Li_2O and Si are taken as the reaction products [27]. Silicon monoxide (SiO) is also lithium reactivity. It has a theoretical capacity over 1400 mA h g^{-1} [28]. SiO_x reacts with lithium, forming Si and Li-oxides of Li_2O, Li_4SiO_4 [29–31] or $Li_2Si_2O_5$ [32] possibly in different mechanisms in the first lithiation process. The products of Li_2O and Li_4SiO_4 are considered irreversible, but $Li_2Si_2O_5$ is reversible [32]. The lithium inactive Li_2O or/and Li_4SiO_4 could serve as a buffer to alleviate the volume expansion of Si in the following cycles, including the Si formed in the first lithiation process of SiO_x. Therefore, SiO_x has theoretically better cycle performance than bare Si [33–35]. SiO_x coated Si nano-tubes were reported had much better cycle performance than the bare Si nano-tubes due to that there was a much stable SEI (solid electrolyte interface) layer formed at the surfaces of the former than at the letter [5].

In this study, submicro-scale a-Si@SiO_x/C composites with a-Si as core and coated with a double layer of SiO_x and carbon were simply synthesized by ball milling c-Si and carbonization of the mixtures of ball-milled Si and citric acid. Different ratios of Si to citric acid were used in order to optimize the composition and structure and thus the electrochemical performance of the composites. Depending on the different carbon contents introduced, floc-like carbon in between the carbon coated a-Si@SiO_x particles and bulk carbon mixed with the a-Si@SiO_x particles exist. The effects of the amorphous structure of Si and the introduction of carbon on the electrochemical property of the composites are systematically investigated. The results show that the composite with a carbon content of *ca.* 8.4 wt.% possesses high electrochemical performance as anode material for LIBs. The fabrication method is considered facile, and is hopefully favorable for large-scale production of submicro-sized Si anode materials.

2. Experimental

As-received commercial Si powder (1–2 μm, 99.99%, ST-nano S&T CO., LTD) without further purifying was ball milled for 100 h under Ar atmosphere by a planetary mill (QM-1SP04, Nanjing University Instrument Plant, China) with a rotation speed of 500 rpm. The as-received Si has an oxygen content of 5.6 wt.% (analyzed by an oxygen analyzer, TC-436, LECO). A ball-to-powder weight ratio of 30:1 was used. The ball-milled Si and citric acid powder (AR, Sinopharm) were mixed in deionized water and followed by a 4-h ultrasonic treatment. Weight ratios of 1/1.25, 1/2.5, 1/3.5, 1/5 and 1/10 of Si to citric acid (powder) were used. The obtained Si and citric acid suspensions were dried at 120 °C in a vacuum oven and then heat-treated at 600 °C for 4 h under a flowing Ar atmosphere to carbonize the citric acid, forming composites. Furnace cooling under argon flow was used.

The crystal structure of the composites was identified by X-ray diffraction (XRD) (X'Pert PRO, PANalytical) using Cu Kα radiation. The microstructure of the composites was characterized by field-emission scanning electron microscopy (FE-SEM, S-4800, Hitachi), transmission electron microscopy (TEM, Tecnai G2 F30, FEI Company) and high resolution TEM (HRTEM). Raman measurement of the composites was performed by a confocal Mirco-Raman spectrometer (inVia-Reflex, Renishaw plc) with 514 nm wavelength incident laser light. The O contents of the composites were analyzed by the TC-436 oxygen analyzer, and the C contents were analyzed by an elemental analyzer (Vario Micro, Elenemtar Analysensysteme GmbH). X-ray photoelectron spectroscope (XPS, ESCALAB 250Xi, Thermo Scientific) equipped with an Al Kα X-ray radiation source (photon energy 1486.6 eV) was used for the analysis of the chemical valence of Si in the SiO_x at the surface of Si particles. The specific surface areas of the Si particles before and after ball milling were measured by the Brunauer–Emmet–Teller (BET) method by nitrogen adsorption isotherms collected at 77 K using a Quantachrome Autosorb analyzer.

The composite electrodes were prepared by coating the slurries consisting of 70 wt.% composite, 20 wt.% conductive agents of acetylene black and vapor growth fiber, and 10 wt.% binder of sodium carboxymethyl cellulose which were dissolved in a buffer solution of citric acid, HCl and NaOH with pH = 3 on a copper foil using a blade coater. The electrodes were dried at 120 °C in vacuum and followed a press at room temperature. The mass loading of the active material was *ca.* 1.5 mg cm^{-2} for each anode. 2025 coin-type cells were assembled in an Ar-filled glove box with lithium metal foil as the counter electrode. A solution of 1 M $LiPF_6$ in 1:1 (wt:wt) of ethylene carbonate and dimethyl carbonate was used as electrolyte. Cells were galvanostatically discharged (lithiation) and charged (delithiation) on a multi-channel battery testing system (NEWARE BTS-610, Neware Technology LTD, China) at 100 and 500 mA g^1, respectively, with a cut-off potential of 0.02–1.50 V vs. Li^+/Li. Cyclic voltammetry (CV) measurement was performed using a multi-channel electrochemical testing system (MATAT, Arbin Instrument) at a scan rate of 0.1 mV s^{-1} and a potential range of 0.005–2 V (vs. Li^+/Li). All electrochemical tests were performed at 25 °C. The specific capacities of the synthesized composites were calculated by taking the total mass of the composites as active material.

In comparison purpose, selected parallel tests were also done for the pristine Si, as-milled Si and the ball-milled Si which was heat treated at 600 °C for 4 h, simulating the heat treatment process of the mixture of the ball-milled Si and citric acid for carbonization.

3. Results and discussion

3.1. Structure characterization

Fig. 1 shows the XRD patterns of the composites prepared from carbonization of the mixtures of the ball-milled Si and citric acid in different weight ratios. For comparison, those of the as-milled Si, ball-milled Si heat treated as well as the pristine Si are also shown. It is seen that the diffraction peaks of Si are significantly broadened and even disappeared after ball milling. There are only two humps occurring around 25–35° and 45–60° in the pattern of the as-milled Si, indicating that the crystal structure of Si is mostly damaged and amorphous structure is formed. For the ball-milled Si further heat treated, there is no visible change in the XRD pattern compared with the as-milled one, expect for the weak diffraction peaks of Si protruding from the humps at around 28 and 47°, indicating that the amorphous structure of Si is mostly retained but with finite re-crystallization after the heat treatment. There is also no visible difference in the XRD patterns of the composites with different citric acid additions and the ball-milled Si heat-treated, indicating that the carbonization process has no detected effect on the crystal structure of Si. There are no distinguishable diffraction peaks of C and SiO_x detected in the XRD patterns, however, the measurements of O and C contents in the composites and the O content in the individual Si (including pristine Si, as-milled Si and the milled Si further heat treated), the results of which are listed in Table 1, demonstrate the existence of amorphous C and SiO_x in the composites and the existence of SiO_x in the individual Si. The Si contents of the samples listed in Table 1 are obtained by subtracting the corresponding O and C.

Si is inevitably oxidized, forming a thin passive SiO_x layer at its surface, in the environmental atmosphere. It is demonstrated from the O contents of the composites (Table 1) that composites composed of SiO_x coated a-Si and C (a-Si@SiO_x/C) are formed after the carbonization process. Moreover, as seen from Table 1, the O content in the as-milled Si is increased to 11.7 wt.% from the

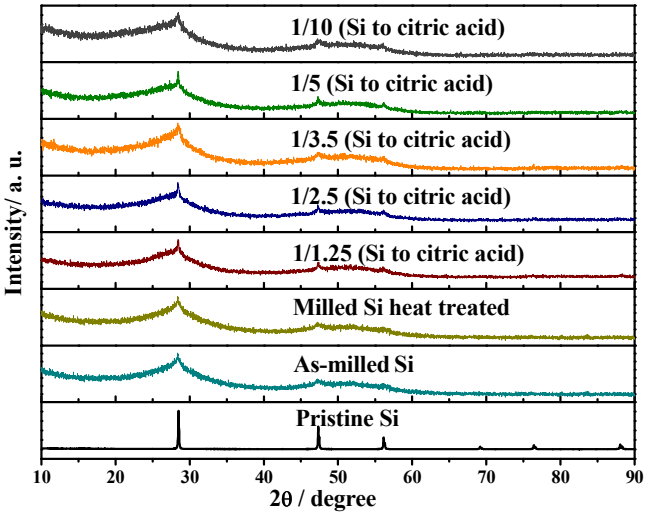

Fig. 1. XRD patterns of the composites prepared from carbonization of the mixture of the ball-milled Si and citric acid in different weight ratios, the as-milled Si, ball-milled Si heat treated as well as pristine Si.

Table 1
Contents of O and C of the Si@SiO_x/C composites prepared from different ratios of Si to citric acid, the pristine Si, as-milled Si, ball-milled Si heat treated, and the contents of their corresponding SiO_x layers.

Samples	Composition/wt.%			Contents of the SiO_x layers[a]/wt.%
	O	C	Si	
Pristine Si	5.6	–	94.4	11.4
As-milled Si	11.7	–	88.3	23.7
Milled Si heat-treated	11.7	–	88.3	23.4
a-Si@SiO_x/C (1/1.25)	11.3	4.8	83.9	22.6
a-Si@SiO_x/C (1/2.5)	10.9	8.4	80.7	21.8
a-Si@SiO_x/C (1/3.5)	10.7	10.4	78.9	21.4
a-Si@SiO_x/C (1/5)	9.9	15.9	74.2	19.8
a-Si@SiO_x/C (1/10)	8.7	24.6	66.7	17.4

[a] The contents of SiO_x are calculated based on the measured O contents and the assumption that the SiO_x layer is homogenously composed of SiO_2 and SiO with the detected ratios obtained from XPS.

5.6 wt.% for the pristine Si. A possible reason is that the ball-milled Si particles have considerable fresh surfaces and surface defects, which facilitate the formation of SiO_x by the reaction of Si with the oxygen in the ambient atmosphere once the samples are taken out from the milling jar. However, the O content is almost not changed for the ball-milled Si after the heat treatment (Table 1). In addition, the O contents in the a-Si@SiO_x/C composites are lower than that in the as-milled Si due to the decreased contents of ball-milled Si in the composites, and a higher carbon content corresponds to a lower O content, as seen in Table 1. The carbon contents in the a-Si@SiO_x/C composites are increased from 4.8 to 24.6 wt.% with the decrease of the ratios of Si to citric acid from 1/1.25 to 1/10. However, the weight ratios of Si to O in the a-Si@SiO_x/C composites with different carbon contents are almost the same, which is also the same as that in the as-milled Si, indicating that the amount of O induced in the ball-milled Si are almost not influenced by the carbonization process.

The change in the structure of Si from crystal to amorphous after ball milling and the almost preserving of the amorphous structure after the heat treatment are further confirmed by Raman measurement. Fig. 2(a) shows the Raman spectra of the as-milled Si, the milled Si heat treated as well as the pristine Si. The sharp peak at *ca.* 520 cm^{-1} of the spectrum of pristine Si corresponds to crystalline Si. A shift towards wavenumber of *ca.* 465 cm^{-1} and a significant broadening for the peaks of the as-milled Si and the heat-treated one confirm the amorphous feature of Si in these two products. The Raman spectra of the a-Si@SiO_x/C composites with different citric acid additions are shown in Fig. 2(b). The broad peak centered at *ca.* 465 cm^{-1} in the as-milled and the heat treated ones is still seen in the composites, confirming the amorphous feature of Si in the composites. The almost same peak position of a-Si in the a-Si@SiO_x/C composites with different citric acid indicates similar structure of Si in the different composites. Moreover, D band around 1350 cm^{-1} and G band around 1590 cm^{-1} of the intrinsic feature of amorphous carbon are visibly seen, providing extra evidence of the existence of amorphous carbon in the composites.

The chemical characteristics of the Si in the SiO_x layers of the pristine Si, as-milled Si and milled Si heat treated determined by XPS are illustrated in Fig. 3. It is seen that there are broad peaks at around 103 eV in all the samples, corresponding to SiO_2 (103.2 eV) and SiO (102.4 eV), demonstrating the existence of SiO_2 and SiO bonds in the SiO_x layer. In addition, comparatively sharp peak at around 99 eV corresponding to Si $2p_{1/2}$ (99.6 eV) and Si $2p_{3/2}$ (99.0 eV) are also observed. The appearance of the Si signal is probably attributed to the individual Si remaining in the SiO_x layer without oxygen insertion or/and from the Si matrix under the SiO_x layer, as the thickness of the SiO_x layer could be slightly less than

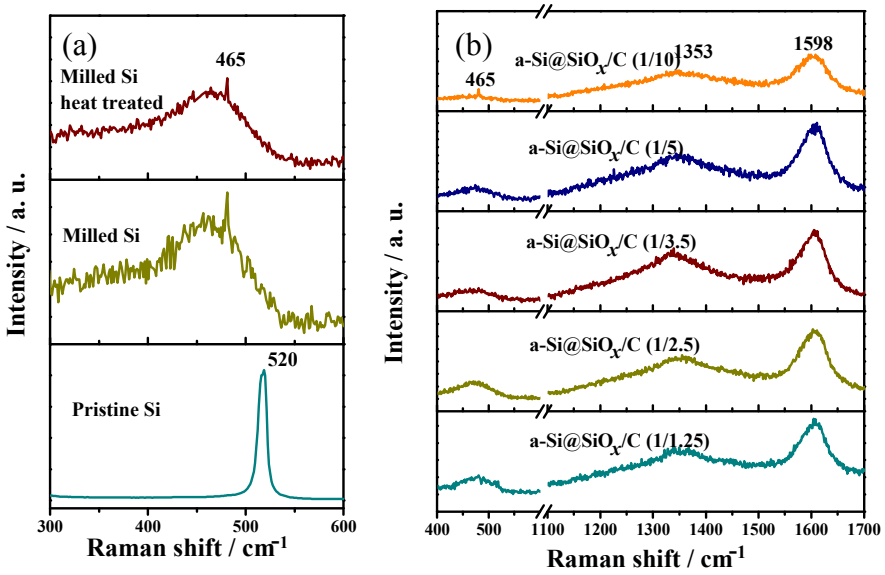

Fig. 2. Raman spectra of the pristine Si, as-milled Si and milled Si heat treated (a), and the a-Si@SiO_x/C composites prepared from different ratios of Si to citric acid (b).

the depth that the X-ray photoelectron could penetrate. By integrating the peak intensities, the contents of SiO_2, SiO and Si in the detected surface layers are obtained and listed in Table 2. It is seen that the contents of SiO_2, SiO and Si of the as-milled Si and the pristine Si are very close. However, the content of SiO is slightly decreased and those of SiO_2 and Si are slightly increased for the ball-milled Si after heat treatment, which is supposed due to the partial decomposition of SiO to Si and SiO_2 in the heat treatment process. If considered roughly that the SiO_x layer was only composed of SiO_2 and SiO with the detected ratio by XPS and the composition along the thickness of the SiO_x layer was homogenous, further combining the O content detected, the contents of SiO_x for the different samples are estimated and also listed in Table 1. It is seen that the content of SiO_x in the pristine Si is around 11 wt.%. However, the value is increased to 23 wt.% after ball milling and the content is almost not changed after the heat treatment. The decrease of the original Si in the composite causes the decrease of the SiO_x content in the composite from 23 to 17 wt.% for the minimum to maximum addition of citric acid.

Fig. 4(a)–(f) shows the SEM images of the pristine Si, as-milled Si and the a-Si@SiO_x/C composites with different Si to citric acid ratios. It is seen that the particle size of Si is evidently reduced from

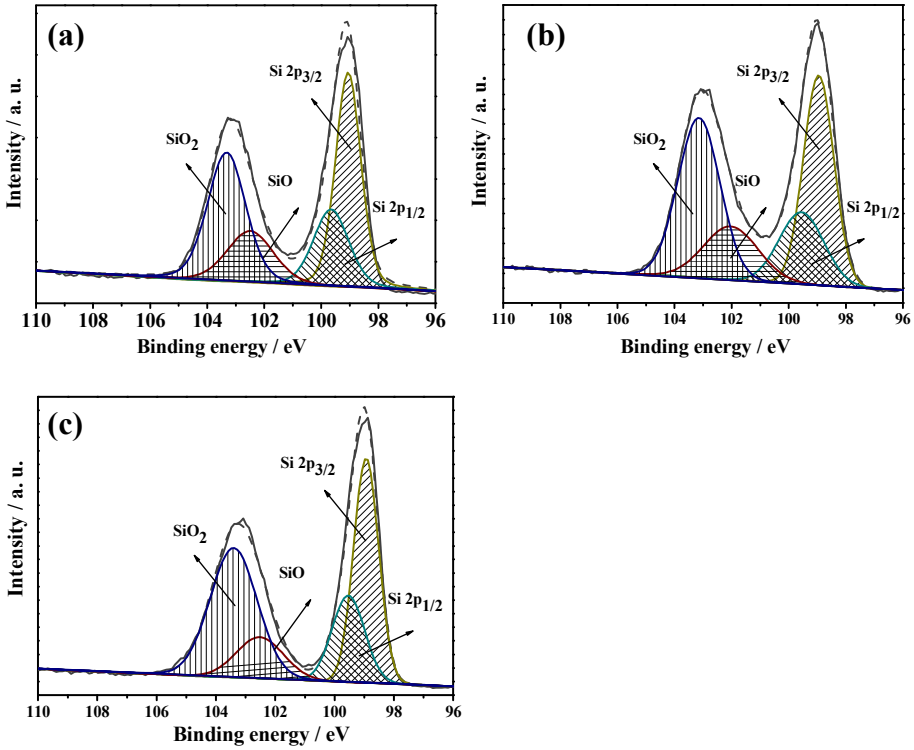

Fig. 3. XPS spectra of Si 2p of the pristine Si (a), as-milled Si (b) and the milled Si heat treated (c).

Table 2
XPS data of the Si 2p of the pristine Si, as-milled Si, milled Si heat treated and the concentration of the corresponding Si, SiO and SiO_2 in the detected layers.

Samples	Phases		Assignment energy/eV	Concentration/mole%
Pristine Si	Si	$Si_{3/2}$	99.0	50.9
		$Si_{1/2}$	99.6	
	SiO_x	SiO	102.4	15.7
		SiO_2	103.2	33.4
As-milled Si	Si	$Si_{3/2}$	99.0	50.0
		$Si_{1/2}$	99.6	
	SiO_x	SiO	102.0	15.1
		SiO_2	103.2	34.9
Milled Si heat treated	Si	$Si_{3/2}$	98.9	50.8
		$Si_{1/2}$	99.5	
	SiO_x	SiO	102.5	11.7
		SiO_2	103.4	37.5

1 to 2 μm for the pristine Si (Fig. 4(a)) to 100–200 nm (Fig. 4(b)) after ball milling, corresponding to an increase in the BET surface area from 7.0 to 22 $m^2\ g^{-1}$. The morphology of the ball-milled Si after the heat treatment at 600 °C shows no visible change, hence, the image is omitted here. For the composites prepared from different Si to citric acid ratios (Fig. 4(c)–(f)), the morphology of the one prepared from the Si to citric ratio of 1/1.25 (Fig. 4(c)), corresponding to a low carbon content of 4.8 wt.% (Table 1), is also not visibly different from that of the as-milled one (Fig. 4(b)). Individual carbon is rarely found in this composite by SEM due to its limited content. The occasionally found individual carbon shows floc-like shape, as circled in Fig. 4(c). With the increasing addition of citric acid, and thus the increasing content of carbon in the composites, carbon is readily found. The individual carbon still appears mostly as floc-like shape when the Si to citric acid ratio is decreased to 1/2.5, corresponding to a carbon content of 8.4 wt.%. Most of the Si particles are well dispersed and are linked by the floc-like carbon, as seen in Fig. 4(d). When the Si to citric acid ratio is decreased to 1/3.5 (10.4 wt.% C), most of the carbon still exists as floc-like shape, as marked by the arrows in Fig. 4(e). However, agglomeration of Si particles embedded in bulk carbon occurs in the area congregating carbon. As seen from Fig. 4(e), large particles appear, though there are still considerable dispersed Si particles with floc-like carbon connecting. When the ratio of Si to citric acid is further decreased to 1/5 (15.9 wt.% C), the agglomeration becomes severe, and considerable Si particles mixed with carbon, forming large particles, as seen from Fig. 4(f). For the composite with Si to citric acid ratio of 1/10, due to the high carbon content (24.6 wt.%), there are more large particles of mixed Si and C. The morphology is omitted here considering the space of the paper.

Fig. 5(a) shows representatively a TEM image of the a-Si@SiO_x/C composites, which is from the one with the Si to citric acid ratio of 1/2.5 (8.4 wt.% C). Carbon coating of the a-Si@SiO_x/C composites cannot be clearly observed by SEM. However, TEM observation (Fig. 5(a)) shows clearly that the Si particles are coated by a thin layer, though the thickness is uneven. The uneven layer is supposed to consist of both SiO_x and C. The circled regions show clearly the floc-like carbon, which connects the Si particles. However, it is hardly to find the exact interfaces of the phases of Si, SiO_x and C, even by HRTEM, as shown representatively in Fig. 5(b), due probably their amorphous feature.

3.2. Electrochemical properties

The voltage profiles of the first discharge/charge at a current density of 100 mA g^1 of the a-Si@SiO_x/C composites with different Si to citric acid ratios are shown in Fig. 6. For comparison, those of the pristine Si, as-milled Si, milled Si heat treated are also shown. The first discharge/charge capacities and the initial Coulombic efficiency of the samples are listed in Table 3. The pristine Si shows the highest discharge and charge capacities of 3960 and 3180 mA h g^{-1}, respectively, corresponding to an initial Coulombic efficiency of 80%. The first discharge and charge capacities of the Si after ball milling are decreased in approximate 500 and 300 mA h g^{-1}, respectively. However, a slightly higher initial Coulombic efficiency of 82% is obtained. It is reported that amorphous Si can accumulate larger amount of Li ions compared to crystalline Si [36] and ball-milled Si shows increasing initial discharge capacity with the increase of the ball-milling time [25]. One of the possible reasons for the lower initial discharge/charge capacities of the as-milled Si than that of the pristine one in the present study is that the former has higher content of SiO_x, corresponding to a lower theoretical capacity.

Fig. 6 shows further that there is a large sloping discharge plateau in the potential range of *ca.* 1.5–0.3 V (vs. Li^+/Li) and a small sloping plateau in the potential range of *ca.* 0.3–0.1 V for the pristine Si, resulting in totally a discharge capacity of approximate

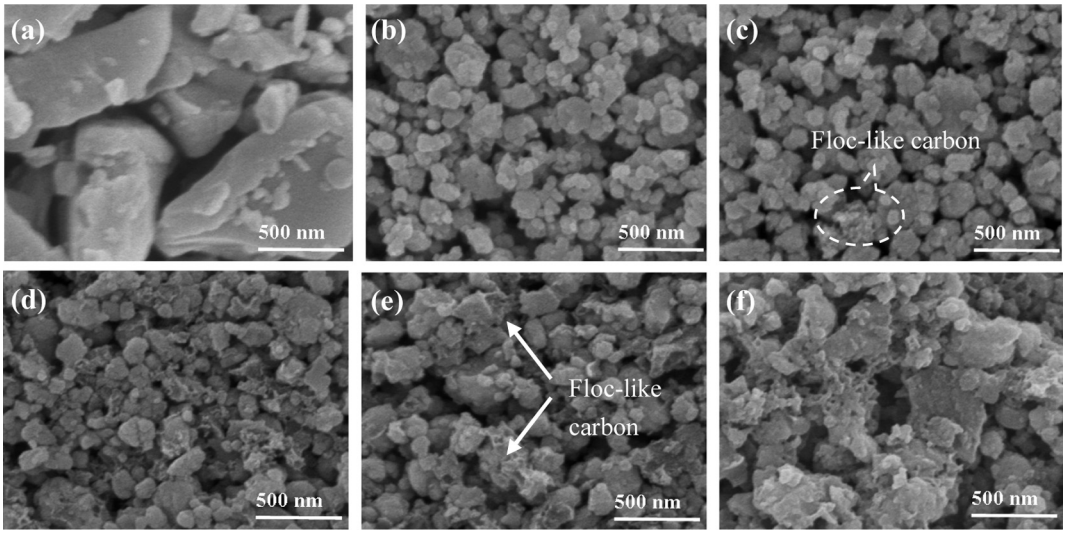

Fig. 4. SEM images of the pristine Si (a), as-milled Si (b) and the a-Si@SiO_x/C composites with Si to citric acid ratios of 1/1.25 (c), 1/2.5 (d), 1/3.5 (e), 1/5 (f).

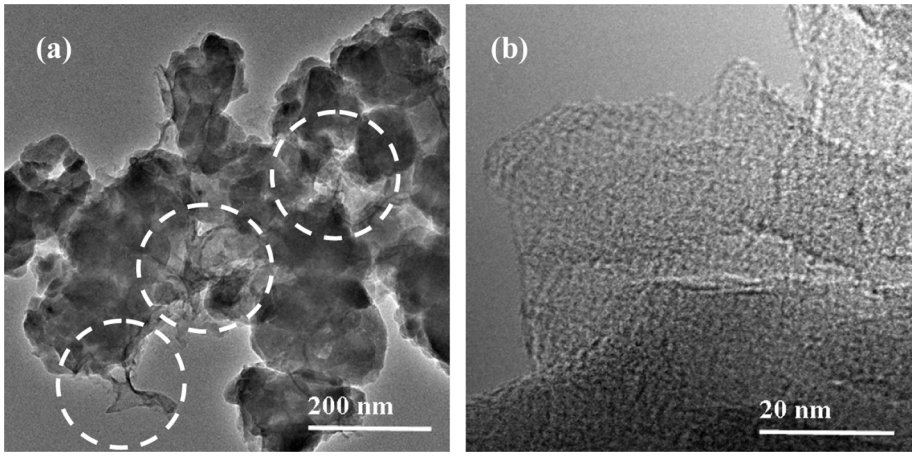

Fig. 5. TEM (a) and HRTEM (b) images of the a-Si@SiO_x/C composite with a Si to citric acid ratio of 1/2.5.

780 mA h g^{-1}. Thereafter, there is an almost flat plateau up to the cut-off voltage of 0.02 V, which corresponds to the typical lithiation of crystal Si. The sloping plateau in the comparatively higher potential range is considered to attribute to the irreversible reactions between the electrode and the electrolyte, and the one in the comparatively lower potential range is associated with the electrolyte decomposition according to previous literature [27]. Meanwhile, for the as-milled Si, a sloping discharge plateau at the high potential range is still visible, but it ends at *ca.* 0.6 V, which is higher than that of the pristine Si. This plateau is also associated with the irreversible reactions between the electrode and the electrolyte. Thereafter, there is a continuously decreased plateau up to the cut-off voltage of 0.02 V for the lithiation of Si. The lithiation of amorphous Si takes place possibly in higher potential range than crystal Si. Moreover, irreversible reactions between the electrode and the electrolyte and the electrolyte decomposition could also occur at the early stage of the discharge plateau. The higher starting potential of lithiation of Si and the slightly larger slope compared with that of the pristine Si demonstrate a different lithiation process for the amorphous Si. For the milled Si further heat treated and the a-Si@SiO_x/C composites, the two-step plateau feature at the high potential range occurring in the pristine Si is not visible, and the one-step high sloping plateau at the high potential range results in smaller capacities compared with the pristine Si and as-milled Si. As the re-crystallization of the ball-milled Si after the heat treatment is limited, the milled Si heat treated and the composites all show typical amorphous lithiation process.

Moreover, as the SiO_x at the surface of the Si particles is amorphous, it is also lithium reaction active as known from previous investigations [11,26,27,37]. It is inferred that the initial irreversible capacities of either the individual Si (including its SiO_x surface layer) or the a-Si@SiO_x/C composites also include those generated by the formation of Li_2O or/and Li_4SiO_4. In addition, the ball-milled Si has much smaller particle size and offers larger surface area compared with the pristine Si for the reaction with electrolyte to form solid electrolyte interface (SEI) layers. Further more, the BET surface area of the as-milled Si is *ca.* three times of that of the pristine one, and the SiO_x content of the former is *ca.* twice of the later (Table 1), which indicate that the average thickness of the SiO_x layer of the as-milled Si is thinner than that of the pristine one. Therefore, it is inferred that the prevention of Si from the direct contact of the electrolyte for the as-milled Si by the SiO_x layer is not much effective than that for the pristine one. In addition, due to the less amount of SiO_x in the pristine Si, the irreversible capacity caused by the irreversible reaction of SiO_x with lithium should also be lower. However, as aforementioned, the initial Coulombic efficiency of the pristine Si is slightly lower than that of the as-milled one. Hence, it seems that crystal Si generates more irreversible capacity from the reaction with electrolyte and the decomposition of electrolyte compared with the amorphous one. Higher initial Coulombic efficiency of the milled Si than crystal Si is also reported by Gauthier et al. [24]. Further more, as seen from Table 3, the heat treatment at 600 °C for the ball-milled Si does not result in measurable difference in the first discharge/charge capacities and the initial Coulombic efficiency, indicating that the limited re-crystallization in the ball-milled Si almost does not influence the initial lithiation and de-lithiation processes.

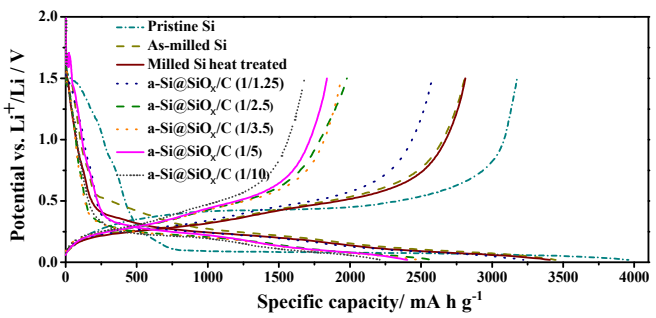

Fig. 6. Voltage profiles of the a-Si@SiO_x/C composites with different ratios of Si to citric acid, the as-milled Si, milled Si heat treated and the pristine Si.

Further seen from Table 3, the first discharge/charge capacities of the a-Si@SiO_x/C composites are lower than those of the three individual Si (Si@SiO_x). The decrease is mainly caused by the introduction of the low-capacity carbon. The a-Si@SiO_x/C composite with 4.8 wt.% C shows first discharge and charge capacities of 3210 mA h g^{-1} and 2580 mA h g^{-1}, respectively. For the composite with carbon contents of 8.4–15.9 wt.%, the discharge and charge capacities are all lowered by 700–800 mA h g^{-1} compared with those of the composite with 4.8 wt.% C. When the carbon content is further increased to 24.6 wt.%, the first discharge and charge capacities are only of 2390 and 1680 mA h g^{-1}, respectively. Further more, the initial Coulombic efficiency of the composite is decreased from 80% to 70% with increasing the carbon content from 4.8 to 24.6 wt.%. It is common that carbon generates high irreversible capacity by the formation of SEI layer. Previous work in our group showed that the amorphous carbon derived from citric acid at 700 °C had only an initial Coulombic efficiency of 54% [38].

Fig. 7(a) and (b) shows the cycling performances of the a-Si@SiO_x/C composites at discharge/charge currents of 100 and 500 mA g^1, respectively. In the case that discharge/charge current of

Table 3
Electrochemical properties of the a-Si@SiO_x/C composites with different Si to citric acid ratios as well as the pristine Si, as-milled Si and milled Si heat treated (discharge/charge current of 100 mA g^{1}).

Samples	1st Discharge capacity/mA h g^{-1}	1st Charge capacity/mA h g^{-1}	1st Columbic efficiency/%	Capacity after 100 cycles/ mA h g^{-1}	Capacity retention after 100 cycles/%
Pristine Si	3960	3180	80	650	20
As-milled Si	3420	2810	82	1060	38
Milled Si heat treated	3430	2810	82	650	23
a-Si@SiO_x/C (1/1.25)	3210	2580	80	1120	43
a-Si@SiO_x/C (1/2.5)	2580	1980	77	1450	73
a-Si@SiO_x/C (1/3.5)	2540	1940	76	1240	64
a-Si@SiO_x/C (1/5)	2410	1840	76	740	40
a-Si@SiO_x/C (1/10)	2390	1680	70	660	39

500 mA g^{1} was used, the composites were initially cycled at 100 mA g^{1} for 5 cycles. For comparison, the cycling performances of the pristine Si, as-milled Si and the milled Si further heat treated are also selectively shown. The capacities and capacity retentions of the samples cycled at 100 mA g^{1} after 100 cycles are also listed in Table 3. It is seem that though the initial reversible capacity of pristine Si is as high as 3180 mA h g^{-1}, a capacity of only 650 mA h g^{-1} is retained after 100 cycles, corresponding to a capacity retention of only 20%. For the as-milled Si, though the initial reversible capacity is lowered to 2810 mAh g^{-1}, the capacity after 100 cycles is much higher, being of 1060 mA h g^{-1}, corresponding to a capacity retention of 38%. Amorphous structure causes less pulverization due to the isotropic expansion during lithium insertion compared with the highly anisotropic expansion of crystalline Si, hence favoring the cycle stability. For the milled Si further heat treated, the capacity after 100 cycles is 670 mA h g^{-1}, corresponding to a capacity retention of 23%, which is still slightly higher than that of the pristine one. The decrease in cycle stability after the heat treatment is suggested due to the slight re-crystallization of Si and also the slight structure changes of the SiO_x layer as shown in Table 2. Although the irreversible Li_2O or Li_4SiO_4 formed from the reaction of SiO_x and lithium can serve as buffer to alleviate the volume expansion of Si [33,35], the present SiO_x in the individual submicro-sized Si is unable to assist the Si anode to get favorable cycle performance.

However, with the in situ introduction of the pyrolyzed amorphous carbon, the cycle stability of the composite is evidently improved. In terms of the effect of the carbon contents, as seen from Table 3, the capacity and capacity retention of the a-Si@SiO_x/C composites after 100 cycles first increase and then decrease with the increase of the carbon contents, reaching a maximum value of 1450 mA h g^{-1} and 73%, respectively, when the carbon content is 8.4 wt.% (the Si to citric acid ratio of 1/2.5). As aforementioned, the in situ introduced carbon occurs as both floc-like shape connecting the a-Si@SiO_x particles, and thin layers coating the a-Si@SiO_x particles. The carbon not only improves the electrical conductivity of the a-Si@SiO_x/C composites but also buffers the volume change of Si during lithium insertion and extraction, thus improves the cycle performance of the composites. However, when the content is low (4.8 wt.%), its improvement in the cycle stability is limited. The composite only possesses a capacity and capacity retention of 1120 mA h g^{-1} and 43% after 100 cycles, respectively. When the carbon content is in the high range of 10.4–24.6 wt.%, the cycle stability is again lowered (Table 3), which is due to the agglomeration of carbon and a-Si@SiO_x particles, forming large mixed particles (Fig. 4). Therefore, it is concluded that fine dispersed a-Si@SiO_x particles and the effective connecting and coating of the carbon are the key factors for the composite to possess superior cycle performance. In addition, the lithium inactive Li_2O or/and Li_4SiO_4 formed from the reaction of SiO_x and lithium in the first lithiation process serve as buffer, alleviating partially the volume expansion of Si, which also favors the cycle performance of the composites. For the cycling performance of the composites at the current density of 500 mA g^{1}, Fig. 7 shows that the variation tendencies of the capacity and capacity retention with the carbon content are consistent with those at current density of 100 mA g^{1}. The a-Si@SiO_x/C composite prepared from the Si to citric acid of 1/2.5 (8.4 wt.% C) also reaches the highest capacity among all the composites, 1230 mA h g^{-1} after 100 cycles, which is 85% of that obtained at the current density of 100 mA g^{1}. If evaluating the capacity retention from the 6th cycle after the initial 5 cycles at 100 mA g^{1}, a capacity retention of 86% after 100 cycles is achieved.

Fig. 8(a)–(h) shows the cyclic voltammetry curves of the electrodes of the pristine Si, as-milled Si, milled Si heat treated and the a-Si@SiO_x/C composites prepared from different Si to citric acid ratios at a scanning rate of 0.1 mV s^{-1} for the first 5 cycles. As shown in Fig. 8(a), the pristine Si has two broad cathodic peaks centered at around 1.4 V (vs. Li^+/Li) as the dominant and 0.8 V (vs. Li^+/Li) as the minor, respectively, in the first cycle, which could be attributed to the formation of SEI on the surface of the electrode by the reaction of the electrode and the electrolyte, and the decomposition of electrolyte, respectively. Cathodic peaks at potentials of 1.3 and

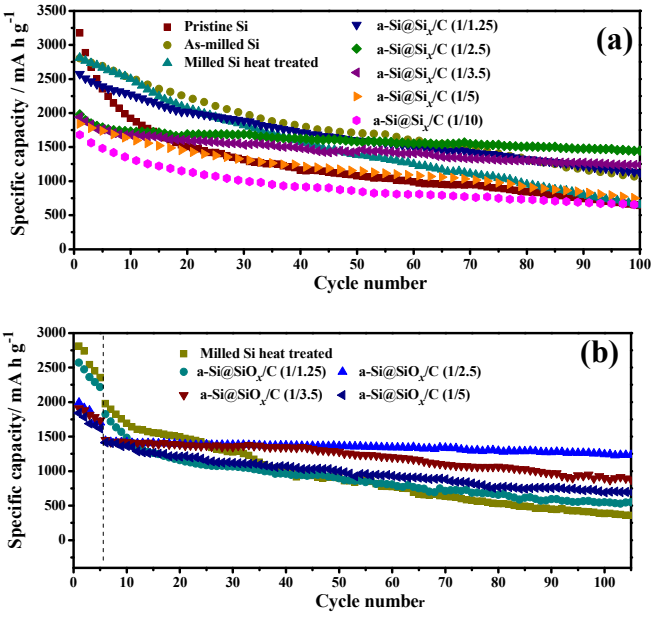

Fig. 7. Cycling performances of the a-Si@SiO_x/C composites with different Si to citric acid ratios as well as the pristine Si, as-milled Si and milled Si heat treated at discharge/charge current densities of 100 mA g^{1} (a) and 500 mA g^{1} (b). For (b), the composites were initially cycled at 100 mA g^{1} for 5 cycles.

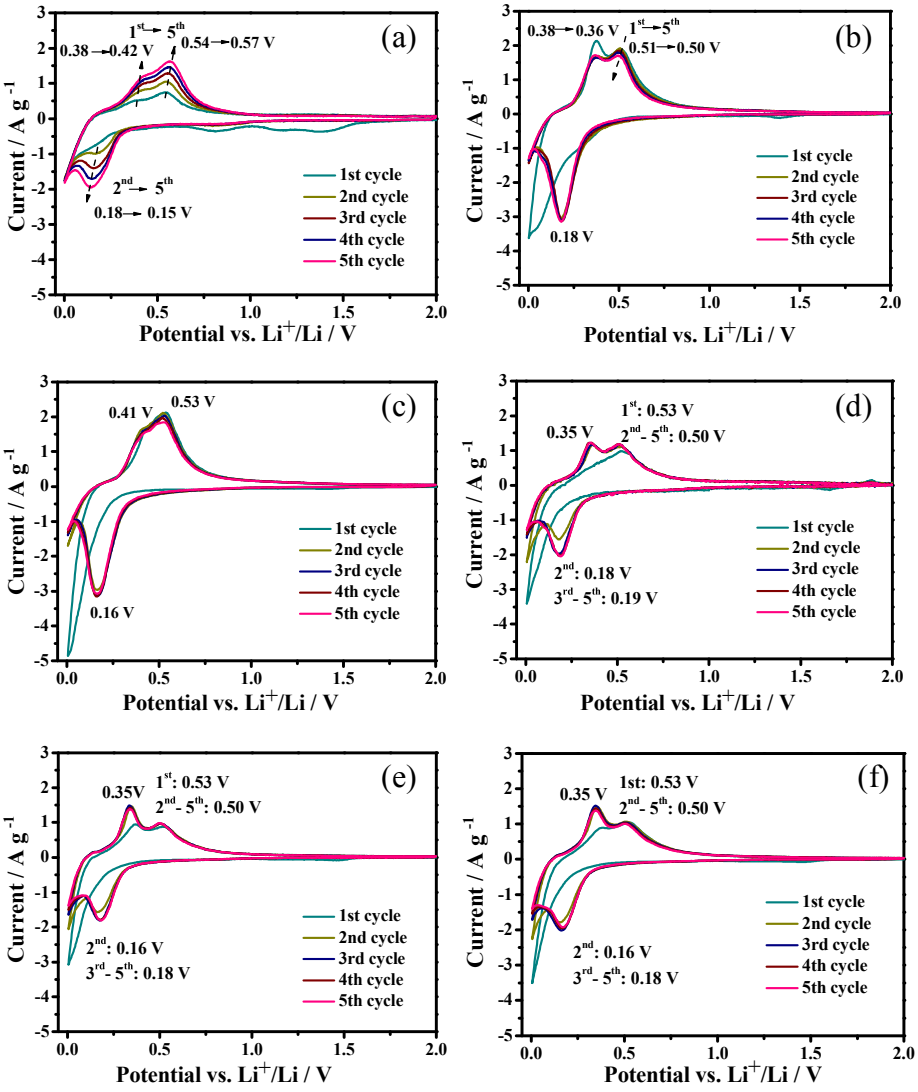

Fig. 8. Cyclic voltammetry profiles of the anodes of the pristine Si (a), as-milled Si (b), mill Si heat treated (c) and the a-Si@SiO_x/C composites prepared from a Si to citric acid ratio of 1/2.5 (d), 1/3.5 (e), 1/5 (f).

0.55 V corresponding to the SEI formation and electrolyte decomposition, respectively, were reported by Yan et al. in a porous SiO_2 nano-cube anode [27]. The appearance of two peaks in the high potential range is also consistent with the occurrence of two sloping plateaus in the corresponding high potential range in the first discharge curve of the sample (Fig. 6). Both peaks disappear after the first cycle, indicating their irreversible feature. However, these two broad cathodic peaks in the first cycle are evidently reduced for all the other samples, especially for one at the comparatively low potential, as seen in Fig. 8(b)–(f), which is also consistent with the phenomenon that there is almost only one discharge plateau in the high potential range, and the plateau is extremely sloping (Fig. 6) for these samples. This phenomenon is also in good agreement with the result that the pristine Si anode has larger irreversible capacity than the others. Fig. 8 further shows that continuous lithiation starts from *ca.* 0.3 V (vs. Li^+/Li) and ends at the cut-off potential (0.005 V) in the first cathodic process for all the samples. Generally, the onset lithiation potentials of SiO_x and carbon are slightly higher than that of Si. Therefore, it is suggested that the lithiation starts firstly from SiO_x and C, and then Si. A high lithiation level is reached when the potential approaches the cut-off one. It is reported that a decrease in potential for lithiation toward 0 V at low intercalation levels could be due to the high concentration of lithium at the surface of the alloy (Li_xSi alloy) grains [39]. The as-milled Si shows the broadest lithiation peak at the potential close to the cut-off one among all the samples, indicating a gradual lithiation process and the lowest concentration of lithium at its surface. Since the second cycle, the intensity of the sharp peak closing to the cut-off potential is greatly reduced and a new broad peak centered at 0.14–0.18 V occurs in all the samples. The peak position and the peak intensity are slightly different for the different samples as seen in Fig. 8(a)–(f). This broad peak is supposed from the formation of metastable Li–Si amorphous phases (Li_xSi) [40,41]. The sharp peak closing to the cut-off potential is attributed to the phase transition of amorphous Li_xSi to crystalline $Li_{15}Si_4$, as it is reported that crystalline $Li_{15}Si_4$ forms at potential below 0.02 V [42], and the present cut-off potential is 0.005 V.

For the anodic process of the first cycle, as an overall, there are two broad peaks in the potential range of 0.34–0.54 V. As the carbon derived from citric acid showed no exact peaks in cathodic and anodic processes [38], and after the first lithiation process, SiO_x converted to Si and Li_2O/Li_4SiO_4, the present anodic peaks are mostly from a two-step lithium extraction process of Li–Si alloy to Si. However, the peak positions are somewhat

different for the different samples due to their different microstructure.

Upon cycling, the broad cathodic peak position of the phase transformation of the Li_xSi with low level intercalation of Li to high level intercalation of Li for pristine Si is decreased from 0.18 to 0.16 V from the 2nd to 5th cycle, meanwhile, the two anodic peak positions are increased from 0.38/0.54 V to 0.42/0.57 V, respectively (Fig. 8(a)). In addition, the intensities of both cathodic and anodic peaks are increased with cycling, which is supposed due to activation, as the pristine Si has large particle size and the sweeping time of the CV process is insufficient for it to reach a full Li-intercalation. Moreover, the increase in the potential difference between the redox peaks of the pristine Si with cycling is visible, indicating a severe polarization. As seen from Fig. 8(b), there is almost no activation upon cycling for the as-milled Si, which is supposed due to the decreased particle size and amorphous structure. In addition, the cathodic and anodic curves are almost overlapped after the 1st cycle, demonstrating a good reversibility. Moreover, the cathodic peaks of the ball-milled Si (located at *ca.* 0.18 V) is slightly higher than those of the pristine Si (0.15–0.18 V), and the two anodic peak potentials (0.36 and 0.50 V) are slightly lower than those of the pristine Si (0.38–0.42 and 0.54–0.57). This indicates that the as-milled Si has better lithium insertion and extraction kinetics, or in other words, less polarization, than the pristine Si. For the milled Si further heat treated (Fig. 8(c)), though the CV curves after the 1st cycle are also almost overlapped, the broad cathodic peak moves to 0.16 V and the anodic peaks move to 0.41 and 0.53 V. The potential difference of the redox peaks (including the sharp cathodic peak closing to the cut-off potential) of the milled Si further heat treated is slightly larger than that of the as-milled one, indicating a slightly larger polarization during cycling, which is attributed to the slight re-crystallization. However, the potential difference of the redox peaks of the milled Si heat treated after 5 cycles is still smaller than that of the pristine Si.

Activation also exists from the 2nd to 3rd cycles in the Si@SiO_x/C composites, as shown typically in Fig. 8(d)–(f), from those with carbon contents of 8.4, 10.8 and 15.9 wt.%. Moreover, the potential of the cathodic peak of the 2nd cycle of the composite with 8.4 wt.% C is 0.18 V, which is higher than those of the composites with 10.8 and 15.9 wt.% C, being 0.16 and 0.14 V, respectively, indicating a better lithiation kinetics for the former. For the following cycles of the 3rd to 5th, the cathodic peaks are located at *ca.* 0.19, 0.18 and 0.16 V for the composites with carbon contents of 8.4, 10.8 and 15.9 wt.%, respectively. It is seen that the shift of the peak position of the composite with 8.4 wt.% C is little smaller than that of the other two. For the first anodic process, the composite with carbon content of 8.4 wt.% shows only one anodic peak at *ca.* 0.53 V (Fig. 8(d)), while there are two distinct anodic peaks at 0.36/0.53 V and 0.37/0.54 V (Fig. 8(e) and (f)), respectively, for the composites with carbon contents of 10.8 and 15.9 wt.%. It is suggested that the lack of the anodic peak in the lower potential range is due to a better electronic contact and a more homogenous lithiation [24]. The more homogenous lithium extraction process of the composite with 8.4 wt.% C in the 1st cycle is attributed to its fine dispersed Si (Si@SiO_x) particles and the improved electronic contact by the introduction of carbon coating and the floc-like carbon. Since the 2nd cycle, this composite also appears a two-step lithium extraction process. However, the lithium extraction processes of the comparatively lithium-rich and lithium-poor Li–Si alloys are almost comparable, which is different from that of the others, that the lithium extraction process from the comparatively lithium-rich Li–Si alloy is the dominant one. In addition, the two anodic peaks at 0.35 and 0.50 V appearing in the different composites are almost repeated from the 2nd to 5th cycles, which are not visibly influenced by the different carbon contents introduced. However, combining the cathodic peaks, the composite with 8.4 wt.% C still has the smallest potential difference of the redox peaks, demonstrating the best lithium reaction kinetics, which is also attributed to the well dispersed Si (Si@SiO_x) particles connected and coated by the high electronic conductive carbon.

4. Conclusions

a-Si@SiO_x/C composites with amorphous Si as core and a double layer of SiO_x and C were successfully synthesized by ball-milling crystal micron-sized Si powder and the in situ introduction of carbon by carbonization of the mixture of citric acid and the ball-milled a-Si. The a-Si powder has a particle size in the range of 100–200 nm and a SiO_x content of *ca.* 24 wt.% after ball milling. The SiO_x content in the as-milled a-Si is increased to a double value of the pristine Si due to the high activity of Si to oxygen in the ambient atmosphere after ball milling. The carbon contents of the composites are increased from 4.8 to 24.6 wt.% with the Si to citric acid weight ratio decreasing from 1/1.25 to 1/10. Besides the carbon coating at the surface of the a-Si@SiO_x, there are also floc-like carbon formed, which connects the a-Si@SiO_x particles. The Si@SiO_x/C composite with 8.4 wt.% C provides an initial reversible capacity of 1980 mA h g^{-1}, and a capacity of 1450 mA h g^{-1} after 100 cycles at current density of 100 mA g^1, and 1230 mA h g^{-1} after 100 cycles at current density of 500 mA g^1, which are much superior than either the individual Si (pristine Si, as-milled Si) or the composites with other contents of carbon. The improved electrochemical property is attributed to the amorphous structure of Si, which results in increasing amount of lithium diffusion paths and decreasing volume changes during lithiation/delithiation; the double layer of SiO_x and C, which further buffers the volume change of a-Si and prevents the agglomeration of Si during cycling; the carbon coating and the floc-like carbon in between the carbon coated-a-Si@SiO_x particles, which provide improved electronic contact of the Si particles. However, high carbon content over 10 wt.% caused agglomeration of the Si@SiO_x and carbon mixture, decreasing the electrochemical property of the composite. The synthesis method is considered facile and attractive for large-scale production of superior Si-based anode materials for LIBs.

Acknowledgments

This work was supported by National Nature Science Foundation for Distinguished Youth Scholars of China (No. 51025102), National Nature Science Foundation of China (No. 51371158), Program for Innovative Research Team in University of Ministry of Education of China (IRT13037) and Key Science and Technology Innovation Team of Zhejiang Province (2010R50013).

References

[1] S. Bourderau, T. Brousse, D.M. Schleich, J. Power Sources 81 (1999) 233–236.
[2] Y.D. Wang, J. Dahn, J. Electrochem. Soc. 153 (2006) A2314–A2318.
[3] B. Koo, H. Kim, Y. Cho, K.T. Lee, N.S. Choi, J. Cho, Angew. Chem. Int. Ed. 51 (2012) 8762–8767.
[4] L.F. Cui, R. Ruffo, C.K. Chan, H.L. Peng, Y. Cui, Nano Lett. 9 (2009) 491–495.
[5] H. Wu, G. Chan, J.W. Choi, I. Ryu, Y. Yao, M.T. McDowell, S.W. Lee, A. Jackson, Y. Yang, L. Hu, Y. Cui, Nat. Nanotechnol. 7 (2012) 310–315.
[6] Y.Q. Zhang, X.H. Xia, X.L. Wang, Y.J. Mai, S.J. Shi, Y.Y. Tang, C.G. Gu, J.P. Tu, J. Power Sources 213 (2012) 106–111.
[7] W. Li, R. Yang, X. Wang, T. Wang, J. Zheng, X. Li, J. Power Sources 221 (2013) 242–246.
[8] S.S. Suh, W.Y. Yoon, C.G. Lee, S.U. Kwon, J.H. Kim, Y. Matulevich, Y.U. Kim, Y. Park, C.U. Jeong, Y.Y. Chan, S.H. Kang, J. Electrochem. Soc. 160 (2013) A751–A755.
[9] X. Chen, K. Gerasopoulos, J. Guo, A. Brown, C. Wang, R. Ghodssi, J.N. Culver, ACS Nano 4 (2010) 5366–5372.
[10] A. Netz, R. Huggins, W. Weppner, Ionics 7 (2001) 433–439.

[11] P. Lv, H. Zhao, J. Wang, X. Liu, T. Zhang, Q. Xia, J. Power Sources 237 (2013) 291–294.
[12] S. Chen, M.L. Gordin, R. Yi, G. Howlett, H. Sohn, D. Wang, Phys. Chem. Chem. Phys. 14 (2012) 12741–12745.
[13] S.M. Jang, J. Miyawaki, M. Tsuji, I. Mochida, S.H. Yoon, Carbon 47 (2009) 3383–3391.
[14] Z. Zhang, M. Zhang, Y. Wang, Q. Tan, X. Lv, Z. Zhong, H. Li, F. Su, Nanoscale 5 (2013) 5384–5389.
[15] I. Kovalenko, B. Zdyrko, A. Magasinski, B. Hertzberg, Z. Milicev, R. Burtovyy, I. Luzinov, G. Yushin, Science 334 (2011) 75–79.
[16] S. Park, J. Lee, N.S. Choi, Energy Environ. Sci. 5 (2012) 7878–7882.
[17] J.Y. Howe, D.J. Burton, Y. Qi, H.M. Meyer, M. Nazri, G.A. Nazri, A.C. Palmer, P.D. Lake, J. Power Sources 221 (2013) 455–461.
[18] S.H. Ng, J. Wang, K. Konstantinov, D. Wexler, S.Y. Chew, Z. Guo, H.K. Liu, J. Power Sources 174 (2007) 823–827.
[19] J. Wang, Y. Tong, Z. Xu, W. Li, P. Yan, Y.W. Chung, Mater. Lett. 97 (2013) 37–39.
[20] S. Ohara, J. Suzuki, K. Sekine, T. Takamura, J. Power Sources 119 (2003) 591–596.
[21] L.Y. Beaulieu, T.D. Hatchard, A. Bonakdarpour, M.D. Fleischauer, J.R. Dahn, J. Electrochem. Soc. 150 (2003) A1457–A1464.
[22] G.A. Tritsaris, E. Kaxiras, S. Meng, E. Wang, Nano Lett. 13 (2013) 2258–2263.
[23] B. Jerliu, L. Dorrer, E. Huger, G. Borchardt, R. Steitz, U. Geckle, V. Oberst, M. Bruns, O. Schneider, H. Schmidt, Phys. Chem. Chem. Phys. 15 (2013) 7777–7784.
[24] M. Gauthier, D. Mazouzi, D. Reyter, B. Lestriez, P. Moreau, D. Guyomard, L. Roue, Energy Environ. Sci. 6 (2013) 2145–2155.
[25] G.B. Cho, S.Y. Choi, J.P. Noh, Y.M. Jeon, K.T. Jung, T.H. Nam, J. Nanosci. Nanotechnol. 11 (2011) 6262–6265.
[26] W.S. Chang, C.M. Park, J.H. Kim, Y.U. Kim, G. Jeong, H.J. Sohn, Energy Environ. Sci. 5 (2012) 6895–6899.
[27] N. Yan, F. Wang, H. Zhong, Y. Li, Y. Wang, L. Hu, Q. Chen, Sci. Rep. 3 (2013) 1568.
[28] Y.J. Chao, X.X. Yuan, Z.F. Ma, Electrochim. Acta 53 (2008) 3468–3472.
[29] B.K. Guo, J. Shu, Z.X. Wang, H. Yang, L.H. Shi, Y.N. Liu, L.Q. Chen, Electrochem. Commun. 10 (2008) 1876–1878.
[30] Q. Si, K. Hanai, T. Ichikawa, M.B. Philipps, A. Hirano, N. Imanishi, O. Yamamoto, Y. Takeda, J. Power Sources 196 (2011) 9774–9779.
[31] H. Kim, M. Seo, M.H. Park, J. Cho, Angew. Chem. Int. Ed. 49 (2010) 2146–2149.
[32] Q. Sun, B. Zhang, Z.W. Fu, Appl. Surf. Sci. 254 (2008) 3774–3779.
[33] S. Sim, P. Oh, S. Park, J. Cho, Adv. Mater. 25 (2013) 4498–4503.
[34] Y.S. Hu, R. Demir-Cakan, M.M. Titirici, J.O. Muller, R. Schlogl, M. Antonietti, J. Maier, Angew. Chem. Int. Ed. 47 (2008) 1645–1649.
[35] L.W. Su, Z. Zhou, M.M. Ren, Chem. Commun. 46 (2010) 2590–2592.
[36] H. Li, X. Huang, L. Chen, G. Zhou, Z. Zhang, D. Yu, Y. Mo, N. Pei, Solid State Ionics 135 (2000) 181–191.
[37] X. Feng, J. Yang, Q. Lu, J. Wang, Y. NuLi, Phys. Chem. Chem. Phys. 15 (2013) 14420–14426.
[38] M.X. Gao, X. Chen, H.G. Pan, L.S. Xiang, F. Wu, Y.F. Liu, Electrochim. Acta 55 (2010) 9067–9074.
[39] S.H. Nguyen, J.C. Lim, J.K. Lee, Electrochim. Acta 74 (2012) 53–58.
[40] M.K. Datta, J. Maranchi, S.J. Chung, R. Epur, K. Kadakia, P. Jampani, P.N. Kumta, Electrochim. Acta 56 (2011) 4717–4723.
[41] M.K. Datta, P.N. Kumta, J. Power Sources 194 (2009) 1043–1052.
[42] Y.M. Kang, S.M. Lee, S.J. Kim, G.J. Jeong, M.S. Sung, W.U. Choi, S.S. Kim, Electrochem. Commun. 9 (2007) 959–964.